Modeling C–H Abstraction Reactivity of Nonheme Fe(IV)O Oxidants with Alkanes: What Role Do Counter Ions Play

ARTICLE *in* JOURNAL OF PHYSICAL CHEMISTRY LETTERS · SEPTEMBER 2011

Impact Factor: 7.46 · DOI: 10.1021/jz201224x

4 AUTHORS:

Deepa Janardanan
Central University of Kerala
22 PUBLICATIONS **560** CITATIONS
SEE PROFILE

Usharani Dandamudi
Central Food Technological Research Institute
27 PUBLICATIONS **310** CITATIONS
SEE PROFILE

Hui Chen
Chinese Academy of Sciences
62 PUBLICATIONS **2,002** CITATIONS
SEE PROFILE

Sason Shaik
Hebrew University of Jerusalem
525 PUBLICATIONS **20,556** CITATIONS
SEE PROFILE

THE JOURNAL OF PHYSICAL CHEMISTRY Letters

LETTER

pubs.acs.org/JPCL

Modeling C−H Abstraction Reactivity of Nonheme Fe(IV)O Oxidants with Alkanes: What Role Do Counter Ions Play?

Deepa Janardanan, Dandamudi Usharani, Hui Chen,† and Sason Shaik*

Institute of Chemistry, The Hebrew University of Jerusalem, 91904 Jerusalem, Israel

Supporting Information

ABSTRACT: It is shown that the addition of ClO_4^- counterions to $[N4PyFeO]^{2+}$ enables us to avoid the anomalies associated with the self-interaction error in DFT and to describe for the first time the entire trajectories for alkane hydroxylation and desaturation by this potent oxidant. The predicted reactivity trends for cyclohexadiene and cyclohexane reproduce the experimentally observed product selectivity and relative ease of oxidation. Furthermore, the advent of this well-behaved oxidant enables us to derive generalizing principles: (a) orbital selection rules that predict transition state structures and (b) the exchange-enhanced reactivity (EER) principle that predicts the dominance of the high-spin state during the entire oxidation process. It is shown that the orbital selection rules and EER principle are general descriptors of the reactivity of metal-oxo systems and appear to be fundamental principles of chemistry.

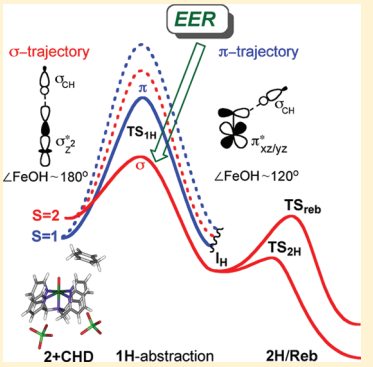

SECTION: Biophysical Chemistry

There is a surge of interest in synthetic models of mononuclear nonheme iron enzymes,[1−6] which perform C−H activation and lead to the formation of alcohols and alkenes. Both the enzymes[1] and the synthetic models utilize high-valent iron(IV)-oxo complexes as the active species.[2−5] One of the potent synthetic complexes is $[N4PyFe^{IV}O]^{2+}$ (N4Py: *N*,*N*-bis(2-pyridylmethyl)-bis(2-pyridyl) methylamine), which is depicted in Scheme 1 and which is capable of activating even cyclohexane.[6,7] However, unlike the enzymatic complexes that have high-spin quintet (S = 2) ground states, the synthetic variants are generally characterized by triplet ground states (S = 1)[4] and low-lying quintet excited states (S = 2) and as such have a more complex reactivity behavior. Density functional theory (DFT) has contributed to the understanding of this reactivity, which was characterized as two-state reactivity (TSR),[8] wherein the S = 2 state cuts through the larger S = 1 barrier and mediates the reaction.[9−13] However, because most of the synthetic complexes carry a high positive charge, usually 2+, the gas-phase calculations have resulted in some nonphysical anomalies, such as barrier-free S = 2 surfaces,[10,11] electron transfer processes, artificial charge delocalization,[14] formation of charged organic intermediates due to hydride abstractions instead of the experimentally observed hydrogen atom abstraction (HAT),[6] and discontinuities in the potential energy profiles.[10,15] These anomalies were invincibly shown[14,16,17] to originate in the self-interaction error inherent in DFT. As such, an important class of these bioinorganic reactions cannot be confidently studied with DFT unless these anomalies can be evaded. Siegbahn et al.[14,16] have suggested that the anomalies can be muted by masking the charge of the iron oxo reagent, for example, by using counterions.[14]

In this Letter, we report the boon of incorporating counterions in the UB3LYP calculations of the reactions, depicted in Scheme 1, of the synthetic complex[6] $[N4PyFe^{IV}O]^{2+}$ with cyclohexadiene, with which all of the above anomalies manifest with the bare oxidant (model **1**), and cyclohexane, for which the anomalies appear after the first HAT, in the follow-up steps in Scheme 1a. As shall be shown, adding the two ClO_4^- counterions (model **2**) as in the $[N4PyFe^{II}(CH_3CN)](ClO_4)_2$ crystal structure[18] removes the anomalies and creates smooth energy profiles that enable one to study the entire stepwise processes in Scheme 1a, explore various reaction trajectories (σ/π)[9b,19−21] of the rate-limiting HAT step, offer unequivocal characterization of the reaction intermediates, assess and derive coherent reactivity

Scheme 1. (a) Reactions Studied Using (b) Oxidant Models 1, 1-solv, and 2 (1-solv Signifies That All Species Are Optimized in the Solvent) and (c) Two Substrates[a]

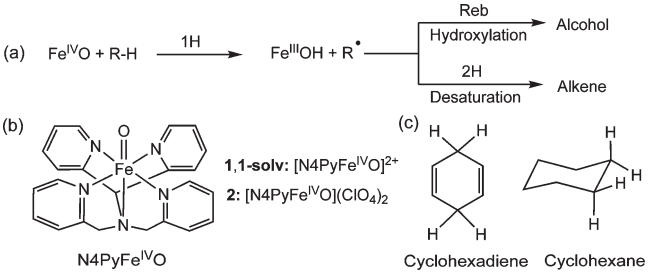

[a] Reb and 2H are abbreviated processes.

Received: September 7, 2011
Accepted: September 26, 2011
Published: September 26, 2011

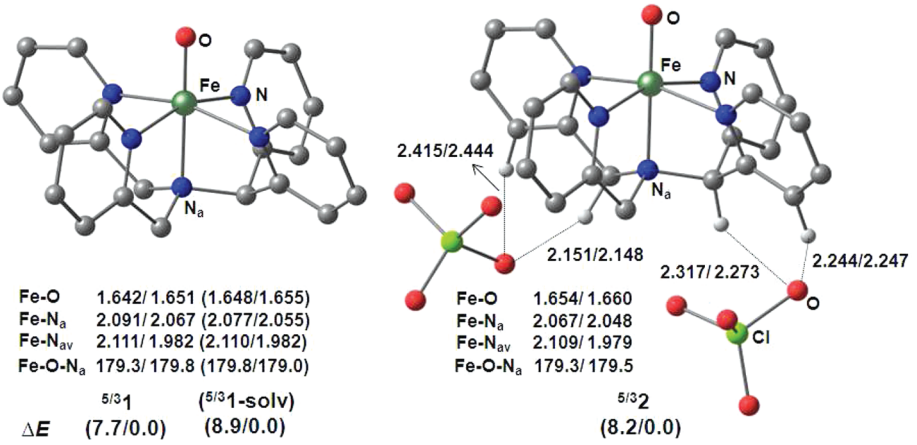

Figure 1. UB3LYP/B1 key geometric parameters and spin-state energy gaps (UB3LYP/B2/B1 for **1**, **1-solv** (with solvation corrections included), and **2** (distances in angstroms, angles in degrees, and energies in kilocalories per mole; hydrogen atoms are not shown for clarity)).

principles for these nonheme reagents, such as the recently proposed exchange-enhanced reactivity (EER) principle,[21−24] and compare the results to experimental finding.[6,7]

These reactions were studied with UB3LYP (see methods), using gas-phase and solvent optimization for the reactions of **1**, which were compared with the reactivity of **2**. The solvent optimization[22,24,25] is supposed to mask at least partially the effects caused by the high positive charge of **1**, and hence the comparison of **1-solv** with addition of the counterions as in **2** will be illuminating. Complete data are available in the Supporting Information (SI) document, whereas key results are presented below.

*Oxidant Models **1** and **2***. Figure 1 shows key geometric features of **1**, **1-solv**, and **2** and their spin-state energy gaps. The positions of counterions in **2** were freely optimized but remained close to those in the crystal structure[18] and remarkably stayed put throughout the reaction pathways. It is seen that the geometric features do not depend much on the conditions of $[N4PyFeO]^{2+}$. As shown in Figure 1, the ground state is $S = 1$, as previously found[9,10,22] and in accord with experiment.[6] However, the spin-state gap of **1** is smaller than that for either **1-solv** or **2**. Therefore, even at the level of oxidant when the charge is unmasked, the high spin state is stabilized to a small extent. As shall be further seen, this little difference increases along the reaction pathway.

*Reactivity of **1** and **2** with Cyclohexadiene*. Figure 2a−c shows the energy profiles for the first H-abstraction step for **1**, **1-solv**, and **2**, whereas Figure 2d shows the follow-up steps to yield alcohol and desaturation products only for **2** (^{5}**P**$_{reb}$ and ^{5}**P**$_{2H}$). Figure 2a exhibits the above-mentioned anomalies; the $S = 2$ state falls spontaneously and generates the intermediate, ^{5}**I**^+_H, which involves a $C_6H_7^+$ cationic species and which seems to be a dead end because we could not generate the benzene product from it. Trying to locate a reactant cluster, ^{5}**RC**, resulted in a spontaneous electron transfer already in this stage (SI, Table S10). Masking the positive charge as in **1-solv** (Figure 2b)[22] improves the situation and reveals both ^{5}**RC** and ^{5}**TS**$_{1H}$ species. The ^{5}**TS**$_{1H}$ species is connected to the ^{5}**I**$_H$ intermediate, which involves a $C_6H_7^\bullet$ radical species. Still, however, ^{5}**I**^+_H is also present as the lowest intermediate. A simple self-interaction error test[14,17] shows that the ^{5}**I**^+_H intermediate is generated from ^{5}**I**$_H$ by electron transfer that becomes complete as the organic moiety gets farther away from the $FeOH^+$ moiety.

By contrast, when the counterions are present, as in Figure 2c, the false ^{5}**I**^+_H intermediate disappears and the barrier on the $S = 2$ state increases, thus indicating that the counterions as in **2** are required to mask the charge, whereas **1-solv** is still insufficient in this respect. Furthermore, as shown in Figure 2d, the follow-up steps proceed exclusively on $S = 2$ wherein ^{5}**I**$_H$ undergoes competitive desaturation and alcohol formation, with a lower barrier for the desaturation to give benzene (which vanishes with dispersion correction).[26−28] This is in accord with experiment wherein only benzene is detected.[29] The solvation-corrected free energy barrier for ^{5}**TS**$_{1H}$, relative to ^{3}**RC**, is 9.5 kcal/mol, and with dispersion correction[26−28] (Figure S4 of the SI) it becomes 10.3 kcal/mol. Adding 4.4 kcal/mol, which is an experimental estimate of $-T\Delta S_{assoc}$ (at $T = 243$ K) for bimolecular association,[22,30] brings the free energy barrier relative to the separate reactants to ∼14 to 15 kcal/mol, close to the experimental value (14.0 kcal/mol).[29]

*Reactivity of **1** and **2** with Cyclohexane*. As expected from a substrate with a high ionization potential (IP)[14] like cyclohexane (IP = 226 vs 203 kcal/mol for cyclohexadiene), the first H-abstraction step with **1** is free of anomalies. The problem resurfaces, however, at the intermediate junction, wherein the ^{5}**I**$_H$ intermediate involves a cyclohexyl radical with a moderately low IP. In the gas phase, ^{5}**I**$_H$ exhibited either a discontinuity or a spike in the conversion steps to cyclohexyl alcohol or to cyclohexene (Figure S1 of the SI). With **1-solv**, ^{5}**I**$_H$ collapses to cyclohexyl alcohol without any barrier (Figure S3 of the SI). Both results are in mismatch with experiment, which revealed the presence of a cyclohexyl radical that could be trapped by O_2,[7] as reported in other cases where the respective radicals were trapped.[13,31] Our tests, confirmed the existence of self-interaction error[14] in ^{5}**I**$_H$, even in the solvent (Table S12, SI).

By contrast, using **2** removes the mismatch with experiment. Figure 3a shows the first H-abstraction step with the characteristic TSR, wherein the $S = 2$ state mediates the reaction. Figure 3b shows the partition of ^{5}**I**$_H$ to cyclohexyl alcohol (^{5}**P**$_{reb}$) and cyclohexene (^{5}**P**$_{2H}$) with a significantly smaller barrier for alcohol formation. The free energy barrier difference (between ^{5}**TS**$_{reb}$ and ^{5}**TS**$_{2H}$) in Figure 3b without solvation correction is 2.9 kcal/mol, whereas with solvation it is 3.9 kcal/mol, and with dispersion correction it becomes 2.3 kcal/mol (Figure S5 of the SI); all values predict minor cyclohexene formation. Solvation lowers the rebound free energy barrier from 4.6 to 1.9 kcal/mol (Figure 3b), values which predict a moderate to short lifetime of the cyclohexyl radical. Furthermore, our calculations show that

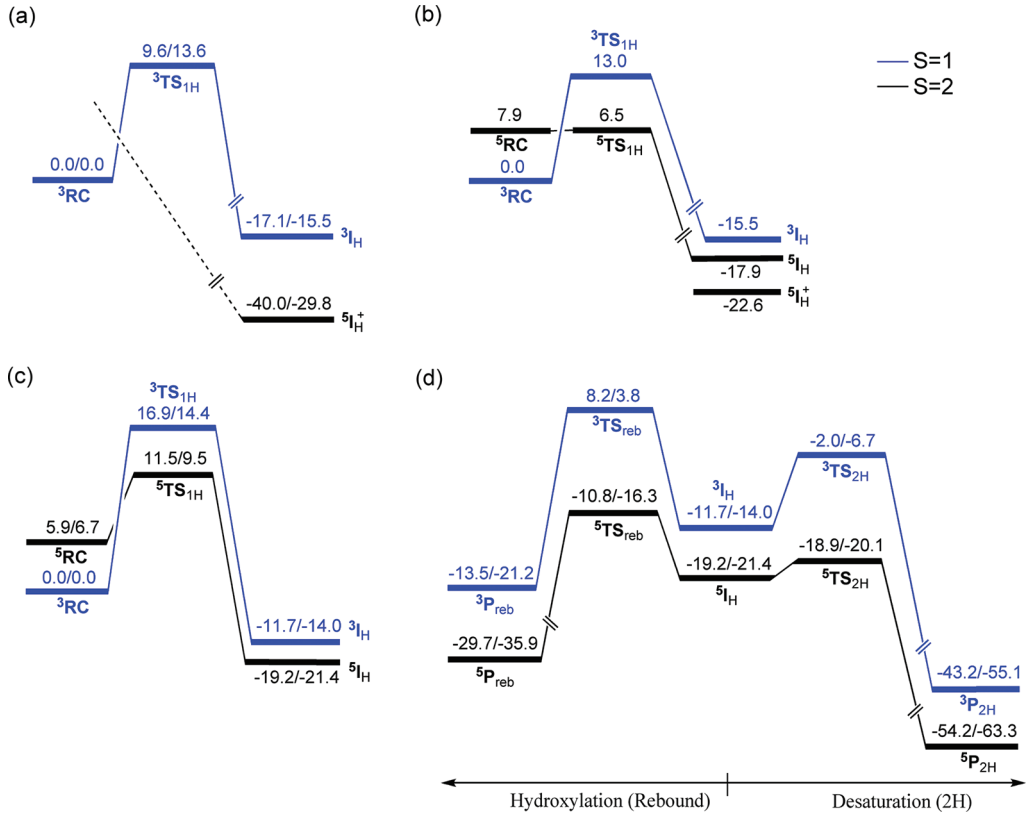

Figure 2. Energy profiles for first H-abstraction step from cyclohexadiene by **1** (a), **1-solv** (b), and **2** (c). The follow-up steps to desaturation and alcohol formation are shown only for **2** (d). All UB3LYP energies are presented in the following order, G/G+solv for **1** and **2** and G+solv for **1-solv**, where G refers to gas-phase free energies at B2. Energy profiles in blue are for $S = 1$ and black are for $S = 2$.

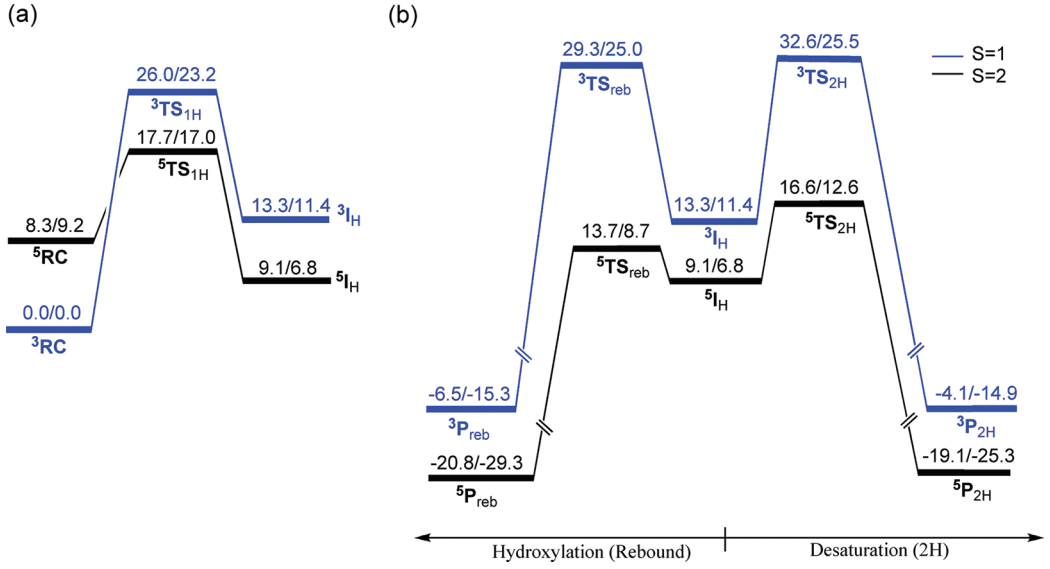

Figure 3. (a) Energy profiles for first H-abstraction step from cyclohexane by **2**. (b) Follow-up steps to desaturation and alcohol formation. All UB3LYP energies are presented in the following order, G/G+solv, where G refers to gas-phase free energies using B2 values. Energy profiles in blue are for $S = 1$ and black are for $S = 2$.

the radical in $^5\mathbf{I}_H$ is weakly bound to the iron-hydroxo species, and dissociation is favored at the free energy scale by −13.0/−6.8 kcal/mol (G+solv/G+solv+D, SI, p S8). Therefore, the formation of a trappable free radical will compete favorably with the rebound and desaturation processes. All in all, this picture is much more consistent with experiment,[6,7] which reveals the formation of cyclohexyl alcohol along with products that are generated by O_2 trapping of the cyclohexyl.[7] Furthermore, the solvation-corrected free energy barrier for $^5\mathbf{TS}_{1H}$ relative to $^3\mathbf{RC}$ is 17 kcal/mol (14.7 with dispersion; Figure S5 of the SI), is significantly larger than the

dx.doi.org/10.1021/jz201224x |J. Phys. Chem. Lett. 2011, 2, 2610–2617

corresponding value for cyclohexadiene, in accord with experimental results.[6,29]

Reactivity Patterns. Rectification of the anomalies by adding counterions enables us to analyze the reactivity patterns of **2** based on a consistent picture. Our focus will be on the first H-abstraction step, which is rate-limiting and which possesses features of significant interest.[2−6,12,14,19−22,24,29,32−39]

TS Trajectories for $^{3,5}TS_{1H}$. Inspection of Figures 2c,d and 3a,b shows that the first H-abstraction follows TSR,[9] wherein the reaction is mediated by the S = 2 state, which dominates all subsequent steps. The S = 1 state that begins as the ground state becomes the excited state starting with the first H-abstraction step, where $^{3}\mathbf{TS}_{1H}$ is significantly higher in energy than $^{5}\mathbf{TS}_{1H}$ for either cyclohexadiene or cyclohexane reacting with **2**. As further shown in Figure 4, $^{3}\mathbf{TS}_{1H}$ has a sideways trajectory with an FeOH angle of ∼126−138°, whereas $^{5}\mathbf{TS}_{1H}$ is virtually upright with an FeOH angle of ∼169−172°. This spin-dependent structural selectivity is common to all oxidant models used herein wherever the two transition states could be located, even though in the presence of the counterions the FeOH angle is about 5−15° larger than in the other models.[9,10] (See Figures S6 and S8 of the SI.)

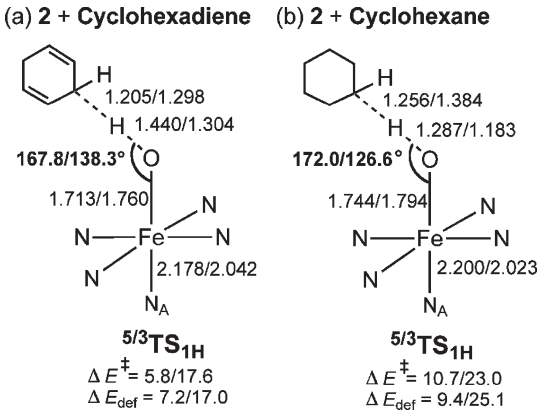

Figure 4. Key geometric features of $^{5}\mathbf{TS}_{1H}/^{3}\mathbf{TS}_{1H}$ for **2** reacting with (a) cyclohexadiene and (b) cyclohexane. Note the FeOH angles. Underneath the TSs, we show the deformation energies of the species and the corresponding gas-phase barriers (relative to the separate reactants, UB3LYP/B2//B1) in kilocalories per mole. Energy data is reported for the S = 2/S = 1 states, in respective order.

Another key feature of the first H-abstraction step is reflected by the total deformation energies, ΔE_{def}, for the two reactants at the respective transition states. Therefore, as specified underneath TS structures, in Figure 4a,b, the ΔE_{def} values are comparable to the corresponding gas-phase barriers. This shows that the barriers derive from the deformations needed to achieve transition states, as frequently found.[40−42] Clearly, these trends in the ΔE_{def} versus the barrier quantities do not show much of a real need to invoke steric effects that destabilize the sideways species, $^{3}\mathbf{TS}_{1H}$, compared with the upright one, $^{5}\mathbf{TS}_{1H}$.

In the absence of clear steric differentiation of the two transition states, the reason for lower energy of $^{5}\mathbf{TS}_{1H}$ compared with $^{3}\mathbf{TS}_{1H}$ requires an explanation. Additionally, the spin-dependent trajectory in $^{5,3}\mathbf{TS}_{1H}$ and the possible link of the trajectories to the relative energy of $^{5,3}\mathbf{TS}_{1H}$ need clarification. Two alternative approaches were proposed to understand the relative TS energies: A frontier molecular orbital approach ascribes the uprightly oriented $^{5}\mathbf{TS}_{1H}$ and its low energy to the favorable orbital interaction between the σ_{CH} orbital of the alkane and the $\sigma^*_{z^2}$ d-orbital compared with a somewhat less favorable σ_{CH}-$\pi^*_{xz/yz}$ interaction in the bent trajectory of $^{3}\mathbf{TS}_{1H}$, which is thought to suffer additionally from steric repulsion[12,33,34] of the alkane with the N4Py ligand (which is not apparent here). An alternative approach, which predicts systematically both the favored trajectory as well as the relative stability of the TSs, uses electron shift diagrams of the type shown in Scheme 2. These diagrams, introduced originally by the Jerusalem group[10,21,37] predict the preferred trajectory based on the orbitals that participate in the electron shift as well as the relative energy of $^{3}\mathbf{TS}_{1H}$ and $^{5}\mathbf{TS}_{1H}$ based on the change in the number of exchange interactions on the metal center during the H-abstraction.

Scheme 2. Electron Shifts Diagrams during the Conversion of $^{5/3}$2/Alkane to the $^{5/3}\mathbf{I}_H$ Intermediates in (a) S = 2 and (b) S = 1[a]

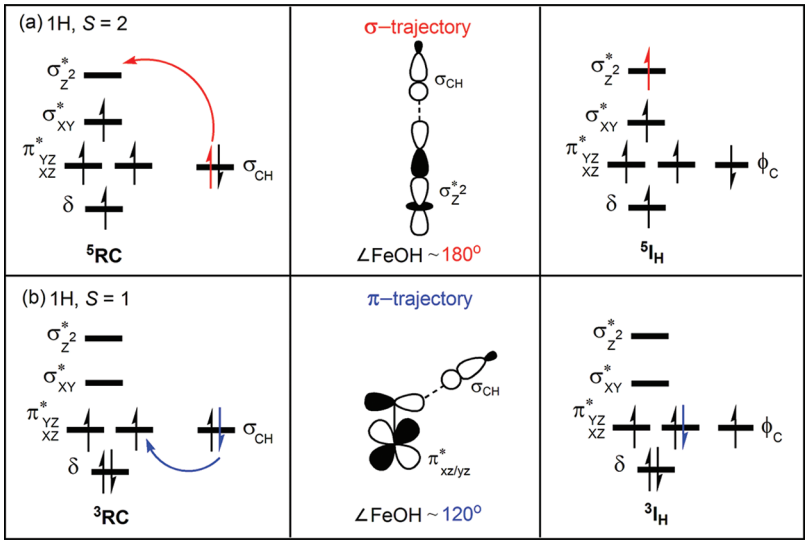

[a] In the middle, we show the orbital-overlap cartoons, which determine the structure of the $^{5,3}\mathbf{TS}_{1H}$ species. The σ and π trajectory labels refer to the acceptor orbitals during the electron shift.

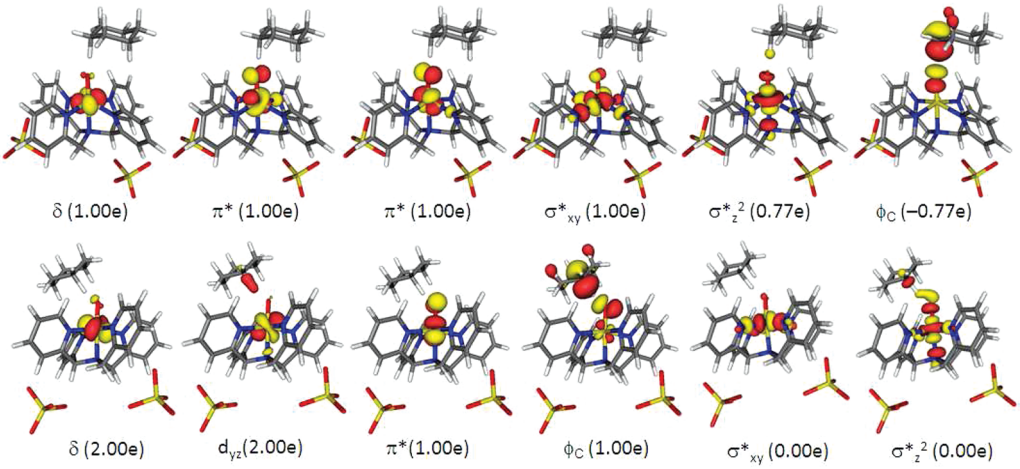

Figure 5. Spin natural orbitals and their occupations in $^{5}\mathbf{TS}_{1H}(\sigma)$ (top panel) for the H-abstraction reaction of **2** with cyclohexane. The negative occupation in ϕ_C signifies a β spin electron. The lower panel shows for $^{3}\mathbf{TS}_{1H}(\pi)$ all natural d orbitals and their occupations.

For clarity, Scheme 2 shows the electron reorganization as the reactants evolve to the intermediates $^{5/3}\mathbf{I}_{H}$, whereas later (Figure 5) we show that the same reorganization operates in the transition states. Scheme 2 reveals that in both $S = 1$ and 2 the d-blocks gain one electron during the H-abstraction and the σ_{CH} bond orbital of the alkane is converted to a singly occupied orbital, ϕ_C, on the alkyl radical. This 1e gain by the d-block is a manifestation of the oxidative nature of the H-abstraction, which can be conceptualized as a proton-coupled electron transfer (PCET) process, whereby the abstracted H atom shifts its electron to the d block while making a bond with a lone pair on the oxygen.[21]

Figure 5 shows that these arguments apply directly to the corresponding transition states $^{5}\mathbf{TS}_{1H}(\sigma)$ and $^{3}\mathbf{TS}_{1H}(\pi)$. Indeed, $^{5}\mathbf{TS}_{1H}(\sigma)$ has ~5 unpaired spin-up electrons in the d-block and a single spin-down electron in an orbital largely located on the alkyl moiety. Therefore, as argued with Scheme 2a, the d-block of $^{5}\mathbf{TS}_{1H}(\sigma)$ gains an electron into the initially vacant $\sigma^*_{z^2}$ orbital, whereas the C−H bond orbital was converted to a singly occupied orbital on the radical moiety with spin down. By contrast, $^{3}\mathbf{TS}_{1H}(\pi)$ has a single spin-up electron in the d block and another one on the alkyl moiety, as argued in Scheme 2b. The gained d electron is now in a d_{yz} orbital that is descendent of the π^*_{yz} orbital of the oxidant in $S = 1$. We emphasize that these electron occupancies in $^{5}\mathbf{TS}_{1H}(\sigma)$ and $^{3}\mathbf{TS}_{1H}(\pi)$ (Figure 5) are fundamental features of electronic structure, which are found for all oxidant models whenever both transition states were available (Figures S13 and S14 of the SI) as well as for other systems previously discussed.[21−23] Furthermore, the extra electron in the d block of the transition states does not manifest without the hydrogen atom. In fact, the electronic structure of the oxidants (**1**, **1-solv**, **2**) with the Fe−O distances elongated to the transition-state distances is precisely identical to the electronic structure of the relaxed oxidants. (See Figures S15 and S16 of the SI.) Therefore, as argued by appeal to Scheme 2, the extra d electron in the d blocks of both transition states transpires because of the PCET that attends the H-abstraction.

Having shown that Scheme 2 is applicable to the corresponding TSs, we proceed to derive orbital-selection rules for the spin-dependent orientational selectivity, in a manner akin to configuration mixing in valence bond theory.[10,21,23,37,38] Therefore, the H-abstraction TS will adopt the geometry that maximizes the overlap of the two orbitals that partake in the electron shift. It is seen from Scheme 2a that in $S = 2$ an α electron is shifted to the $\sigma^*_{z^2}$ d orbital. Therefore, the preferred geometry of $^{5}\mathbf{TS}_{1H}(\sigma)$ will be the one that optimizes the $\sigma_{CH}-\sigma^*_{z^2}$ overlap. As can be seen from the overlap cartoon in Scheme 2a, an upright orientation of $^{5}\mathbf{TS}_{1H}(\sigma)$ will maximize this overlap and dictate the preferred trajectory of the transition state. By comparison to $S = 2$, in $S = 1$, a β-electron shifts to one of the $\pi^*_{xz/yz}$ d orbitals, and accordingly, the overlap cartoon shows that the preferred structure of $^{3}\mathbf{TS}_{1H}(\pi)$ should involve a sideways orientation of the alkane relative to the iron oxo moiety. These selection rules are quite powerful and are obeyed for most if not all of the cases studied by the community.

Exchange Enhanced Reactivity (EER) during the First H Abstraction. Inspection of Figures 2c and 3a shows that unlike $S = 1$, which is bumpy with free energy barriers of 14.4 and 23.2 kcal/mol, the $S = 2$ surface is extremely flat featuring low free energy barriers of 2.7 kcal/mol for cyclohexadiene and 7.8 kcal/mol for cyclohexane. To understand this large difference between the two states, we turn to derive the EER concept,[21] which was first articulated in 2005 for H-abstraction in cytochrome P450.[23] Therefore, because of the particular electron shift in $S = 2$, the d block of $^{5}\mathbf{TS}_{1H}(\sigma)$ now contains five α-electrons, and the number of exchange interactions increases by four exchange terms (4K), relative to the $S = 2$ iron-oxo that has only four spin-identical electrons. By comparison, in $S = 1$, where a β-electron shifts to the $\pi^*_{xz/yz}$ d orbital, the exchange stabilization of $^{3}\mathbf{TS}_{1H}(\pi)$ is downsized by 1K relative to the $S = 1$ iron oxo reactant. The excess exchange stabilization (by 10K terms) of $^{5}\mathbf{TS}_{1H}(\sigma)$ versus $^{3}\mathbf{TS}_{1H}(\pi)$ overcomes the orbital energy gap ($\pi^*_{xz} \rightarrow \sigma^*_{z^2}$) and places $^{5}\mathbf{TS}_{1H}(\sigma)$ and the $S = 2$ intermediate below the corresponding $S = 1$ species. Furthermore, the large exchange enhancement in $S = 2$ flattens this energy profile. Figures 2 and 3 show that these are indeed the computed results. Therefore, $^{5}\mathbf{TS}_{1H}(\sigma)$ is stabilized because of EER,[10,21−24] whereas the $^{3}\mathbf{TS}_{1H}(\pi)$ is raised because of its depleted exchange stabilization. Consequently, the exchange enhancement in $S = 2$ establishes a lower energy $^{5}\mathbf{TS}_{1H}(\sigma)$ with a small deformation energy of the reactants.[43] By contrast, with the exchange depletion, $^{3}\mathbf{TS}_{1H}(\pi)$ is formed with a larger deformation energy and a higher barrier. Steric effects[12,33,34,44] in $^{3}\mathbf{TS}_{1H}(\pi)$ may further augment this difference, but these effects are obviously not manifested in the present systems.

Scheme 3. Electron Shift Diagrams for the Evolution of the Alternative H-Abstraction Transition States in $S = 1$ and $S = 2$[a]

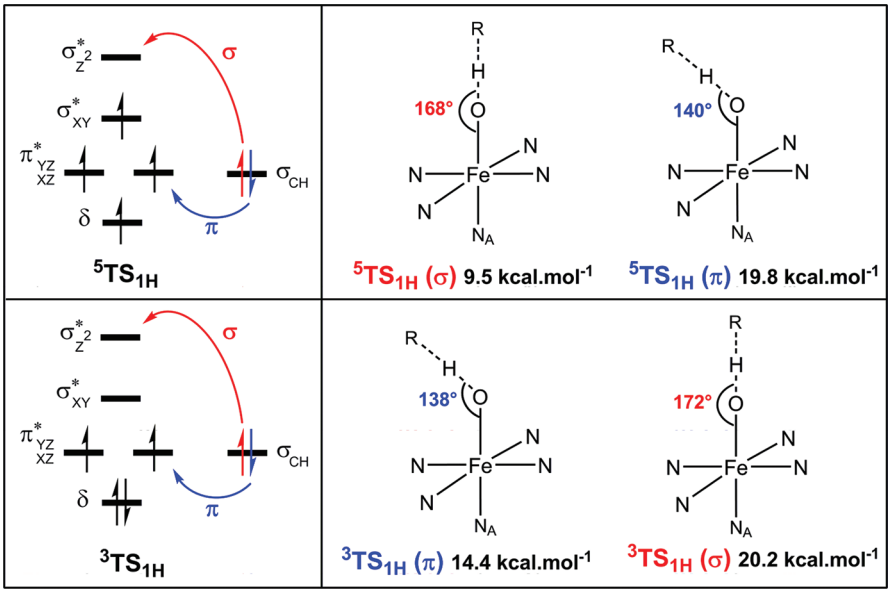

[a] Right-hand column shows schematically the trajectories of the corresponding transition states for **2** + cyclohexadiene and their free energies (G+solv, UB3LYP/B2//B1) relative to the lowest ^{3}**RC** cluster (Figure 2c).

The role of exchange in analogous transition states was nicely demonstrated by Siegbahn et al.[14] by varying the amount of exact exchange in the functional (Figure S17, SI). The concept was extended by de Visser to account for the relative ordering of the transition states during bond activation by the iron-oxo species of the enzyme TauD.[35,36] An equivalent statement of EER was made by Baerends,[12] who ascribed to the low energy of ^{5}**TS**$_{1H}(\sigma)$ to the stabilization of the $\sigma^*_{z^2}$ orbital by exchange-field of the $S = 2$ state.

The advent of the well-behaved oxidant **2**, allows us also to explore the remaining alternative H-abstraction trajectories, via ^{5}**TS**$_{1H}(\pi)$ and ^{3}**TS**$_{1H}(\sigma)$, and hence to test the predictive power of the orbital selection rules and of the EER notion.

To these ends, we explored all trajectories for cyclohexadiene with **2**, as done before by Neese et al. for the reactions of model iron-oxo complexes with ethane.[19] Scheme 3 shows four possible electron shifts and resulting transition states, which are generated by shifting either an α or a β electron to the d block for each spin state. Therefore, for example, unlike ^{5}**TS**$_{1H}(\sigma)$, which is generated by a shift of an α electron to $\sigma^*_{z^2}$ and assumes an upright trajectory, ^{5}**TS**$_{1H}(\pi)$ is generated by a β-electron shift to $\pi^*_{xz/yz}$,[9b] resulting in a sideways trajectory. Because the exchange stabilization of ^{5}**TS**$_{1H}(\pi)$ is reduced by 7K terms, one can predict that ^{5}**TS**$_{1H}(\pi)$ will be higher than ^{5}**TS**$_{1H}(\sigma)$.[9b] Similarly, ^{3}**TS**$_{1H}(\sigma)$ involves an α electron shift from σ_{CH} to $\sigma^*_{z^2}$ and hence the transition is upright.[19,20] ^{3}**TS**$_{1H}(\sigma)$ enjoys only 2K stabilization, which is counterbalanced by a larger destabilization due to the orbital promotion ($\pi^*_{xz/yz} \rightarrow \sigma^*_{z^2}$) relative to ^{3}**TS**$_{1H}(\pi)$, and hence the energy of ^{3}**TS**$_{1H}(\sigma)$ should be higher compared with ^{3}**TS**$_{1H}(\pi)$.[21] The relative energy of the four transition states follows the order: ^{5}**TS**$_{1H}(\sigma)$< ^{3}**TS**$_{1H}(\pi)$ < ^{5}**TS**$_{1H}(\pi)$ < ^{3}**TS**$_{1H}(\sigma)$. This order shows that the transition state that maximizes the number of exchange interactions, namely, ^{5}**TS**$_{1H}(\sigma)$, is the favored one compared with all other possibilities that possess lower exchange stabilization.

Scheme 4. (a) Electron-Shift Diagrams for the Rebound (Reb) and Desaturation (2H) Processes Nascent from ^{5}I$_H$ and Overlap Cartoon and (b) Computed Fe−O−C and Fe−O−H Angles for the Processes in Cyclohexadiene/Cyclohexane in Respective Order

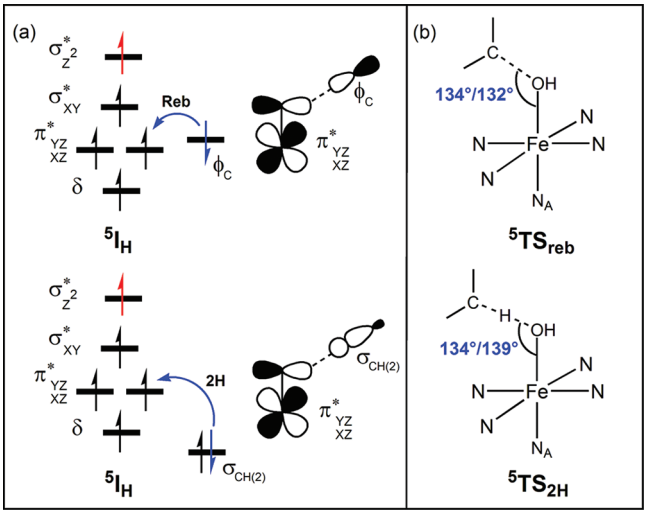

The reactivity of N4PyFeO^{2+} with alkanes is therefore dominated by EER, much like many other systems.[21,22]

Selection Rules for the Follow-Up Steps. The advent of **2** enables us to conclude that the trends in the consecutive steps (2H and reb) by this +2 charged oxidant follow previous results that were previously derived for neutral oxidants.[45] Therefore, here too, the 2H/reb competition is determined by intrinsic properties of the constituents of the $\mathbf{I}_H$ intermediate, $[N4PyFe^{III}OH]^{2+}/R^{\bullet}$, favoring desaturation for cyclohexadienyl and rebound for cyclohexyl. Furthermore, the orbital selection rules predict the

dx.doi.org/10.1021/jz201224x |J. Phys. Chem. Lett. 2011, 2, 2610–2617

structure of the corresponding transition states ^{5}**TS**$_{reb}$ and ^{5}**TS**$_{2H}$. Now the selection rules for the two spin states are reversed and the high spin processes involve sideways trajectories[45] because the respective electron shifts transpire from the ϕ_C orbital of the radical (for rebound) or from the $\sigma_{CH(2)}$ orbital of the adjacent C−H bond (for desaturation) to the π^* orbital of Fe^{III}OH, as shown in Scheme 4. As such, ^{5}**TS**$_{reb}$ will assume the structure that optimizes the ϕ_C−π^* overlap, whereas the ^{5}**TS**$_{2H}$ will optimize the $\sigma_{CH(2)}$-π^* overlap. These selection rules are met in the sideways trajectory for both processes. Scheme 4b shows that these predictions are manifested in the computed Fe−O−C and Fe−O−H angles of ^{5}**TS**$_{reb}$ and ^{5}**TS**$_{2H}$.

In summary, the addition of counterions to $[N4PyFeO]^{2+}$ enables us to avoid the anomalies associated with the self-interaction error, as suggested,[14] and to describe for the first time the entire trajectories for alkane hydroxylation and desaturation for this potent oxidant.[6] Furthermore, the advent of this well-behaved oxidant enables us to test reactivity patterns and derive generalizing principles: (a) orbital selection rules which predict transition state structures and (b) the EER principle that predicts the dominance of the high-spin state during the entire oxidation process. As detailed in our recent work,[21,45] the orbital selection rules and EER principle are quite general descriptors of the reactivity of metal-oxo systems and appear to be fundamental principles of chemistry.[21]

COMPUTATIONAL METHODOLOGY

Geometries of **1** and **2** and species incurred in their reactions with cyclohexadiene and cyclohexane were optimized with Jaguar 7.6[46] with UB3LYP[47−49] and the LACVP[50,51] basis set (UB3LYP/LACVP, denoted as B1). The highest energy points on the reaction pathway scans were used for subsequent search of transition states. The **1-solv** optimizations (B1 level) used the Poisson−Boltzmann solver[52,53] in Jaguar using acetonitrile as solvent (ε = 37.5, probe radius = 2.183 Å). Frequency calculations were performed for all species using Gaussian 03[54] to ascertain the nature of stationary points.

Energies were corrected by single-point calculations using the LACV3P+* basis set (B2). Further corrections included zero-point energy and free-energy corrections, from G03 frequency calculations. As in a previous paper,[45] adding dispersion corrections,[26] was found to have small effects on the barriers (Figures S4 and S5 of the SI). These effects did not change the relative energies of **TS**$_{1H}$ for S = 1 and 2. One should note that in other cases[27,28,55] dispersion correction is highly significant. Spin natural orbitals for ^{5}**TS**$_{1H}$ reproduce the spin density and are available using the keyword pop=spinnatural (Gaussian program).

ASSOCIATED CONTENT

Supporting Information. Full citation of Gaussian03, energy profiles, geometries, orbital pictures, absolute energies, Mulliken spin, charges, and optimized Cartesian coordinates of all stationary points. This material is available free of charge via the Internet at http://pubs.acs.org.

AUTHOR INFORMATION

Corresponding Author

*E-mail: sason@yfaat.ch.huji.ac.il.

Present Addresses

[†]CAS Key Laboratory of Photochemistry, Institute of Chemistry, Chinese Academy of Sciences (ICCAS), Beijing 100190, China.

ACKNOWLEDGMENT

S.S. is supported by the Israel Science Foundation (ISF grant 53/09).

REFERENCES

(1) Krebs, C.; Galonić-Fujimori, D.; Walsh, C. T.; Bollinger, J. M., Jr. Non-Heme Fe(IV)−Oxo Intermediates. *Acc. Chem. Res.* **2007**, *40*, 484–492.

(2) Que, L., Jr. The Road to Non-Heme Oxoferryls and Beyond. *Acc. Chem. Res.* **2007**, *40*, 493–500.

(3) Nam, W. High-Valent Iron(IV)−Oxo Complexes of Heme and Non-Heme Ligands in Oxygenation Reactions. *Acc. Chem. Res.* **2007**, *40*, 522–531.

(4) Shan, X.; Que, L., Jr. High-Valent Nonheme Iron-Oxo Species in Biomimetic Oxidations. *J. Inorg. Biochem.* **2006**, *100*, 421–433.

(5) Bautz, J.; Bukowski, M.; Kerscher, M.; Stubna, A.; Comba, P.; Lienke, A.; Münck, E.; Que, L., Jr. Formation of an Aqueous Oxoiron(IV) Complex at pH 2−6 from a Nonheme Iron(II) Complex and H_2O_2. *Angew. Chem., Int. Ed.* **2006**, *45*, 5681–5684.

(6) Kaizer, J.; Klinker, E. J.; Oh, N. Y.; Rohde, J.-U.; Song, W. J.; Stubna, A.; Kim, J.; Münck, E.; Nam, W.; Que, L., Jr. Nonheme Fe^{IV}O Complexes That Can Oxidize the C-H Bonds of Cyclohexane at Room Temperature. *J. Am. Chem. Soc.* **2004**, *126*, 472–473.

(7) Klinker, E. J. Ph.D. Thesis, Chapter 3, University of Minnesota, 2007.

(8) Schröder, D.; Shaik, S.; Schwarz, H. Two-State Reactivity as a New Concept in Organometallic Chemistry. *Acc. Chem. Res.* **2000**, *33*, 139–145.

(9) Kumar, D.; Hirao, H.; Que, L., Jr.; Shaik, S. Theoretical Investigation of C-H Hydroxylation by (N4Py)Fe^{IV}=O^{2+}: An Oxidant More Powerful than P450? *J Am. Chem. Soc.* **2005**, *127*, 8026–8027.(b) See also Table S5 in the SI.

(10) Hirao, H.; Kumar, D.; Que, L., Jr.; Shaik, S. Two-State Reactivity in C-H Hydroxylation by Non-Heme Iron Oxo Complexes. *J. Am. Chem. Soc.* **2006**, *128*, 8590–8606.

(11) Hirao, H.; Que, L., Jr.; Nam, W.; Shaik, S. A TSR Rationale for the Counterintuitive Axial Ligand Effect on the C-H Activation Reactivity of Nonheme Fe(IV)=O Oxidants. *Chem.—Eur. J.* **2008**, *14*, 1740–1756.

(12) Bernasconi, L.; Louwerse, M. J.; Baerends, E. J. The Role of Equatorial and Axial Ligands in Promoting the Activity of Non-Heme Oxidoiron(IV) Catalysts in Alkane Hydroxylation. *Eur. J. Inorg. Chem.* **2007**, 3023–3033.

(13) Comba, P.; Rajaraman, G. Epoxidation and 1,2-Dihydroxylation of Alkenes by a Nonheme Iron Model System − DFT Supports the Mechanism Proposed by Experiment. *Inorg. Chem.* **2008**, *47*, 78–93.

(14) Johansson, A. J.; Blomberg, M. R.; Siegbahn, P. E. M. Quantum Chemical Modeling of the Oxidation of Dihydroanthracene by the Biomimetic Nonheme Iron Catalyst $[(TMC)Fe^{IV}(O)]^{2+}$. *J. Phys. Chem. C* **2007**, *111*, 12397–12406.

(15) Hirao, H.; Chen, H.; Carvajal, M. A.; Wang, Y.; Shaik, S. Effect of External Electric Fields on the C-H Bond Activation Reactivity of Nonheme Iron-Oxo Reagents. *J. Am. Chem. Soc.* **2008**, *130*, 3319–3327.

(16) Lundberg, M.; Siegbahn, P. E. M. Quantifying the Effects of the Self-Interaction Error in DFT: When Do the Delocalized States Appear? *J Chem. Phys.* **2005**, *122*, 224103.

(17) Johansson, A. J.; Blomberg, M. R.; Siegbahn, P. E. M. Quantifying the Effects of the Self-Interaction Error in DFT: When Do the Delocalized States Appear? II. Iron-Oxo Complexes and Closed-Shell Substrate Molecules. *J. Chem. Phys.* **2008**, *129*, 154301.

(18) Roelfes, G.; Lubben, M.; Chen, K.; Ho, Y. N. R.; Meetsma, A.; Genseberger, S.; Hermant, R. M.; Hage, R.; Mandal, S. K.; Young, V. G., Jr.; et al. Iron Chemistry of a Pentadentate Ligand That Generates a Metastable Fe^{III}-OOH Intermediate. *Inorg. Chem.* **1999**, *38*, 1929–1936.

(19) Geng, C.; Ye, S.; Neese, F. Analysis of Reaction Channels for Alkane Hydroxylation by Nonheme Iron(IV)−Oxo Complexes. *Angew. Chem., Int. Ed.* **2010**, *49*, 5717–5720.

(20) Wang, Y.; Han, K. Steric Hindrance Effect of the Equatorial Ligand on Fe(IV)O and Ru(IV)O Complexes: a Density Functional Study. *J. Biol. Inorg. Chem.* **2010**, *15*, 351–359.

(21) Shaik, S.; Chen, H.; Janardanan, D. Exchange-Enhanced Reactivity: A General Concept in Bond Activation by Metal-Oxo Enzymes and Synthetic Reagents. *Nat. Chem.* **2011**, *3*, 19–27.

(22) Janardanan, D.; Wang, Y.; Schyman, P.; Que, L., Jr.; Shaik, S. The Fundamental Role of Exchange-Enhanced Reactivity in C−H Activation by *S* = 2 Oxo Iron(IV) Complexes. *Angew. Chem., Int. Ed.* **2010**, *49*, 3342–3345.

(23) Hirao, H.; Kumar, D.; Thiel, W.; Shaik, S. Two-States and Two More in the Mechanisms of Hydroxylation and Epoxidation by P450. *J. Am. Chem. Soc.* **2005**, *127*, 13007–13018.

(24) Cho, K. B.; Shaik, S.; Nam, W. Theoretical Predictions of a Highly Reactive Non-Heme Fe(IV)═O Species with a High-Spin Ground State. *Chem. Commun.* **2010**, *46*, 4511–4513.

(25) Seo, M. S.; Kim, N. H.; Cho, K.-B.; So, J. E.; Park, S. K.; Clemancy, M.; Garcia-Serras, R.; Latour, J.-M.; Shaik, S.; Nam, W. A Mononuclear Nonheme Iron(IV)-Oxo Complex Which Is More Reactive than Cytochrome P450 Model Compound I. *Chem. Sci.* **2011**, *2*, 1039–1045.

(26) Grimme, S. Semiempirical GGA-Type Density Functional Constructed with a Long-Range Dispersion Correction. *J. Comput. Chem.* **2006**, *27*, 1787–1799.

(27) Siegbahn, P. E. M.; Blomberg, M. R. A.; Chen, S.-L. Significant van der Waals Effects in Transition Metal Complexes. *J. Chem. Theory Comput.* **2010**, *6*, 2040–2044.

(28) Lonsdale, R.; Harvey, J. N.; Mulholland, A. J. Inclusion of Dispersion Effects Significantly Improves Accuracy of Calculated Reaction Barriers for Cytochrome P450 Catalyzed Reactions. *J. Phys. Chem. Lett.* **2010**, *1*, 3232–3237.

(29) England, J.; Martinho, M.; Farquhar, E. R.; Frisch, J. R.; Bominaar, E. L.; Munck, E.; Que, L., Jr. A Synthetic High-Spin Oxoiron(IV) Complex: Generation, Spectroscopic Characterization, and Reactivity. *Angew. Chem., Int. Ed.* **2009**, *48*, 3622–3626.

(30) Ritchie, C. D. *Physical Organic Chemistry: The Fundamental Concepts*; Marcel Dekker: NY, 1990. See p 132 on experimental values for standard entropy of association.

(31) Bukowski, M. R.; Comba, P.; Lienke, A.; Limberg, C.; Lopez de Laorden, C.; Mas-Balleste, R.; Merz, M.; Que, L., Jr. Catalytic Epoxidation and 1,2-Dihydroxylation of Olefins with Bispidine−Iron(II)/H_2O_2 Systems. *Angew. Chem., Int. Ed.* **2006**, *45*, 3446–3449.

(32) Neidig, M. L.; Decker, A.; Choroba, O. W.; Huang, F.; Kavana, M.; Moran, G, R.; Spencer, J. B.; Solomon, E. I. Spectroscopic and Electronic Structure Studies of Aromatic Electrophilic Attack and Hydrogen-Atom Abstraction by Non-Heme Iron Enzymes. *Proc. Natl. Acad. Sci. U.S.A.* **2006**, *103*, 12966–12973.

(33) Decker, A.; Rohde, J.-U.; Klinker, E. J.; Wong, S. D.; Que, L., Jr.; Solomon, E. I. Spectroscopic and Quantum Chemical Studies on Low-Spin Fe^{IV}═O Complexes: Fe−O Bonding and Its Contributions to Reactivity. *J. Am. Chem. Soc.* **2007**, *129*, 15983–15996.

(34) Ye, S.; Neese, F. Nonheme Oxo-Iron(IV) Intermediates Form an Oxyl Radical upon Approaching the C−H Bond Activation Transition State. *Proc. Natl. Acad. Sci. U.S.A.* **2011**, *108*, 1228–1233.

(35) de Visser, S. P. Propene Activation by the Oxo-iron Active Species of Taurine/α-ketoglutarate Dioxygenase (TauD) Enzyme. How Does the Catalysis Compare to Heme-Enzyme? *J Am. Chem. Soc.* **2006**, *128*, 9813–9824.

(36) Latifi, R.; Bagherzadeh, M.; de Visser., S. P. Origin of the Correlation of the Rate Constant of Substrate Hydroxylation by Nonheme Iron(IV)−Oxo Complexes with the Bond-Dissociation Energy of the C−H Bond of the Substrate. *Chem.—Eur. J.* **2009**, *15*, 6651–6662.

(37) Shaik, S.; Hirao, H.; Kumar, D. Reactivity of High-Valent Iron Oxo Species in Enzymes and Synthetic Reagents: A Tale of Many States. *Acc. Chem. Res.* **2007**, *40*, 532–542.

(38) Chen, H.; Lai, W. Z.; Shaik, S. Exchange-Enhanced H-Abstraction Reactivity of High-Valent Non-Heme Iron(IV)-Oxo from Coupled Cluster and Density Functional Theories. *J. Phys. Chem. Lett.* **2010**, *1*, 1533–1540.

(39) Balcells, D.; Clot, E.; Eisenstein, O. C−H Bond Activation in Transition Metal Species from a Computational Perspective. *Chem. Rev.* **2010**, *110*, 749–823.

(40) van Zeist, W.-J.; Bickelhaupt, F. M. The Activation Strain Model of Chemical Reactivity. *Org. Biomol. Chem.* **2010**, *8*, 3118–3127.

(41) Ioffe, A.; Shaik, S. Intramolecular Effects in the Cycloaddition of Three Ethylenes vs. the Diels-Alder Reaction. *J. Chem. Soc., Perkin. Trans. 2* **1992**, 2101–2108.

(42) Ess, D. H.; Houk, K. N. Theory of 1,3-Dipolar Cycloadditions: Distortion/Interaction and Frontier Molecular Orbital Models. *J. Am. Chem. Soc.* **2008**, *130*, 10187–10198.

(43) When the deformation energy is large, as in ^{5}**TS**$_{1H}$ for **1-solv** with CHD, the exchange enhancement simply lowers the **TS**$_{1H}$ energy and thereby creates a low barrier. See Table S2 of the SI.

(44) Michel, C.; Baerends, E. J. What Singles out the FeO^{2+} Moiety? A Density-Functional Theory Study of the Methane-to-Methanol Reaction Catalyzed by the First Row Transition-Metal Oxide Dications $MO(H_2O)_p^{2+}$, M = V-Cu. *Inorg. Chem.* **2009**, *48*, 3628–3638.

(45) Usharani, D.; Janardanan, D.; Shaik, S. Does the TauD Enzyme Always Hydroxylate Alkanes, While an Analogous Synthetic Nonheme Reagent Always Desaturates Them? *J. Am. Chem. Soc.* **2011**, *133*, 176–179.

(46) *Jaguar*, version 7.6; Schrödinger, LLC: New York, 2008.

(47) Becke, A. D. Density-Functional Thermochemistry. I. The Effect of the Exchange-Only Gradient Correction. *J. Chem. Phys.* **1992**, *96*, 2155–2160.

(48) Becke, A. D. Density-Functional Thermochemistry. III. The Role of Exact Exchange. *J. Chem. Phys.* **1993**, *98*, 5648–5652.

(49) Lee, C.; Yang, W.; Parr, R. G. Development of the Colle-Salvetti Correlation-Energy Formula into a Functional of the Electron Density. *Phys. Rev. B* **1988**, *37*, 785–789.

(50) Hay, J. P.; Wadt, W. R. Ab Initio Effective Core Potentials for Molecular Calculations. Potentials for K to Au Including the Outermost Core Orbitals. *J. Chem. Phys.* **1985**, *82*, 299–310.

(51) Friesner, R. A.; Murphy, R. B.; Beachy, M. D.; Ringlanda, M. N.; Pollard, W. T.; Dunietz, B. D.; Cao, Y. X. Correlated Ab Initio Electronic Structure Calculations for Large Molecules. *J. Phys. Chem. A* **1999**, *103*, 1913–1928.

(52) Tannor, D. J.; Marten, B.; Murphy, R.; Friesner, R. A.; Sitkoff, D.; Nicholls, A.; Ringnalda, M.; Goddard, W. A., III; Honig, B. Accurate First Principles Calculation of Molecular Charge Distributions and Solvation Energies from Ab Initio Quantum Mechanics and Continuum Dielectric Theory. *J. Am. Chem. Soc.* **1994**, *116*, 11875–11882.

(53) Marten, B.; Kim, K.; Cortis, C.; Friesner, R. A.; Murphy, R. B.; Ringnalda, M. N.; Sitkoff, D.; Honig, B. New Model for Calculation of Solvation Free Energies: Correction of Self-Consistent Reaction Field Continuum Dielectric Theory for Short-Range Hydrogen-Bonding Effects. *J. Phys. Chem.* **1996**, *100*, 11775–11788.

(54) Frisch, M. J.; Trucks, G. W.; Schlegel, H. B.; Scuseria, G. E.; Robb, M. A.; Cheeseman, J. R.; Montgomery, J. A., Jr.; Vreven, T.; Kudin, K. N.; Burant, J. C. et al. *Gaussian03*, revision C.02; Gaussian, Inc.: Wallingford, CT, 2003. See the Supporting Information for full citation of G03.

(55) Lai, W. Z.; Shaik, S. Can Ferric-Superoxide Act as a Potential Oxidant in P450cam? QM/MM Investigation of Hydroxylation, Epoxidation, and Sulfoxidation. *J. Am. Chem. Soc.* **2011**, *133*, 5444–5452.